Werk

Jahr: 1985
Kollektion: fid.geo
Signatur: 8 Z NAT 2148:56
Digitalisiert: Niedersächsische Staats- und Universitätsbibliothek Göttingen
Werk Id: PPN1015067948_0056
PURL: http://resolver.sub.uni-goettingen.de/purl?PPN1015067948_0056

LOG Id: LOG_0022
LOG Titel: Crustal structure beneath the Swabian Jura, SW Germany, from seismic refraction investigations
LOG Typ: article

Übergeordnetes Werk

Werk Id: PPN1015067948
PURL: http://resolver.sub.uni-goettingen.de/purl?PPN1015067948
OPAC: http://opac.sub.uni-goettingen.de/DB=1/PPN?PPN=1015067948

Contact

Niedersächsische Staats- und Universitätsbibliothek Göttingen
Georg-August-Universität Göttingen
Platz der Göttinger Sieben 1
37073 Göttingen
Germany
Email: gdz@sub.uni-goettingen.de

J Geophys (1985) 56:69–80

Journal of Geophysics

Crustal structure beneath the Swabian Jura, SW Germany, from seismic refraction investigations*

D. Gajewski and C. Prodehl
Geophysical Institute, University of Karlsruhe, Hertzstr. 16, D-7500 Karlsruhe 21, Federal Republic of Germany

Abstract. As part of multidisciplinary investigations, combined refraction and reflection seismic experiments were carried out in the area of the geothermal anomaly of Urach, southwest Germany, in 1978 and 1979. Ten refraction and two reflection seismic profiles were recorded which reached maximum distances between 20 and 150 km.

This report presents a detailed velocity-depth model of crust and uppermost mantle, based on the available seismic refraction data. On all profiles a clear P_g phase with velocity 5.6 km/s is observed refracted within the uppermost crystalline basement. On some profiles the P_g phase is followed by a retrograde reflected or diving wave which has an apparent velocity of 6.1 km/s. The amplitudes of the corresponding prograde phase decrease considerably or disappear completely at shotpoint distances greater than 50 km. It is caused by a low-velocity zone with a mean velocity of 5.8 km/s extending from 8 to 19 km in depth and over more than 100 km in horizontal direction along the main profile parallel to the strike of the Swabian Jura. The lower boundary of the low-velocity zone is determined by a reflected phase which varies in quality depending on the inclination of the reflecting boundary. The western boundary of this low-velocity zone is located near the north-eastern edge of the Hohenzollerngraben. To the east it disappears west of the Nördlinger Ries. The structure of the crust southwest of the area containing the low-velocity zone is quite different from the structure towards the NE. The Moho is a first-order discontinuity dipping from 25 km depth in the SW to 26.5 km in the NE. Within the uppermost mantle high velocities ($\geqq 8.4$ km/s) and strong velocity gradients are observed. A gravity investigation suggests high densities for the area of the low-velocity zone. This may be caused by fluid or gas phases or partially molten material, an explanation which is also supported by shear-wave observation.

Key words: Crustal structure – Swabian Jura – Urach geothermal anomaly – Seismic refraction – Low-velocity zone

Introduction

As part of a multidisciplinary investigation of the geothermal anomaly of Urach in southwest Germany, including the 3334-m-deep drillhole Urach 3 (Haenel, 1982), detailed seismic reflection and refraction experiments were carried out in July 1978 and May 1979. Figure 1 shows the location of 10 seismic refraction lines varying in length from 20 to 150 km. The map of Fig. 15 shows the position of two detailed seismic reflection lines which were combined with special wide-angle observations. A description of the seismic refraction experiment and its data preparation is given by Jentsch (1980) and Jentsch et al. (1982). The reflection experiment and its interpretation are described by Bartelsen et al. (1982) and Meissner et al. (1982), the wide-angle survey of the same line by Trappe (1983).

The main purpose of the seismic refraction experiment was to determine depth contours, structure and velocity of the crystalline basement and to investigate whether the causes of the Urach geothermal anomaly might be located within the uppermost 5 km of the crust and whether the resolution of the velocity determination might be accurate enough (Jentsch et al., 1982; Prodehl et al., 1982). Accordingly, the shotpoints were arranged such that an optimal coverage, as well as several 20- to 30-km-long reverse lines, resulted in an average station spacing of 1–2 km.

Some of the profiles were extended to observation distances beyond 100 km, but beyond 30 km the station spacing was 4–5 km on average. In general, the quantity of data is sufficient to allow a quite detailed interpretation. However, it is evident that the arrangement of shotpoints and profiles may not be ideal for investigations of the whole crust because there is no properly reversed long profile and only a few profiles overlap for 30 km at most. As a consequence, the resulting model (see Fig. 6) is not unique, but there are other possible solutions which cannot be ruled out with the data available.

Geology

The geothermal anomaly of Urach is located southeast of Stuttgart at the northern margin of the Swabian Jura. The anomaly has an oval shape, its long axis being directed from WSW to ENE as shown in Fig. 1 by isolines of the geothermal gradient after Carlé (1974).

The whole area of the Urach geothermal anomaly and its surroundings is covered by Mesozoic sediments. The long axis of the anomaly runs parallel to the so-called "Albtrauf", an erosional escarpment formed by the abrupt northern termination of the 300- to 500-m-thick Malm plate (Upper Jurassic limestones) which forms the Swabian Jura

* Contribution No. 275 (55/SFB 108), Geophysical Institute, University of Karlsruhe

Offprint requests to: C. Prodehl

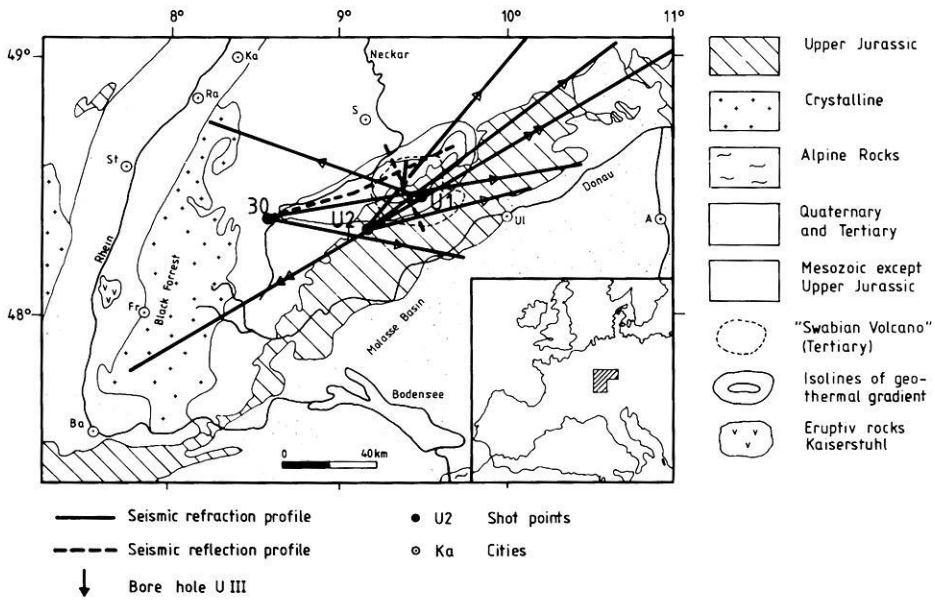

Fig. 1. Geological sketch map of southwest Germany showing the position of the seismic surveys in the area of the Urach geothermal anomaly. Cities: A Augsburg, Ba Basel, Fr Freiburg, Ka Karlsruhe, Ra Rastatt, S Stuttgart, St Strasbourg, Ul Ulm

mountains proper. This escarpment divides the area of investigation: the Swabian Jura in the south with maximum elevations of 850 m above sea level and the foreland to the north (Middle and Lower Jurassic and Triassic sediments) with maximum elevations of 450 m. More than 300 volcanic conduits (upper Miocene) of the so-called Swabian Volcano (Geyer and Gwinner, 1968; Mäussnest, 1974) have perforated the Mesozoic cover of this area. The basement consists mainly of granites and gneisses of the Variscan orogeny and has been found in some drillholes between 1 and 2 km depth below the surface, e.g. at 1.6 km depth in the Urach 3 drillhole mentioned above (Dietrich, 1982; Schädel, 1982).

The rise of the Black Forest and the Vosges in the west accompanied by the formation of the Rhinegraben and the subsidence of the Molasse Basin, i.e. the Alpine northern foreland, in the south are the most important tectonic features in the immediate neighbourhood of the South German Triangle within which the Urach geothermal anomaly is located.

One of the important fracture zones of the area of investigation is the (northwesterly striking) Hohenzollerngraben (Illies, 1982), which is also the site of major earthquake activity since the beginning of this century (Schneider, 1971; Turnovsky and Schneider, 1981) along a south-north trending line cutting through the Hohenzollerngraben near the crossing point of our main seismic refraction line, approximately 20 km WSW of shotpoint U2 (Fig. 1).

Correlation and interpretation of phases

As examples of the data recorded, the record sections of the four profiles U2-60, U1-60, U1-240 and U2-240 are shown in Figs. 2–5. U1 and U2 are shotpoints (Fig. 1), the number 60 or 240 is the azimuth of the corresponding profile. All records are normalized, i.e. the maximum amplitude of any record within the time window shown is scaled to a fixed width. With the exception of a few traces, the signal-to-noise ratio is generally sufficient. The travel-time curves shown in Figs. 2–5 are recalculated from the model shown in Fig. 6. The phases are named in the same manner as that used by other authors (e.g. Giese et al., 1976; Prodehl, 1979).

For the distance range of the first 30 km from the shotpoints, where a very close station spacing was achieved, only selected traces have been plotted in the record sections of the long profiles as shown in Figs. 2–5. The detailed sections for this part are reproduced by Jentsch (1980). They were used for the correlation of phases concerning this distance range (see also Jentsch et al., 1982).

The arrivals a_0 belong to diving waves which travel in the sedimentary layers only. The apparent velocities vary from 3.8–4.2 km/s. With the data available it is not possible to deduce the fine structure of the sediments, but rather the existence of a gradual velocity increase with increasing depth was assumed. The phase a_0 is followed by a phase a_0' in secondary arrivals which corresponds to a reflection from the crystalline basement underlying the sediments.

Beyond 8 km distance the first arrivals belong to the P_g phase, here named a_1, which travels in the uppermost part of the crystalline basement. It gives velocities $\geqq 5.6$ km/s and can be correlated up to 30–40 km shotpoint distance. Jentsch et al. (1982) have used this phase for a time-term analysis in order to derive a depth contour map of the basement for the area of the Urach geothermal anomaly (Jentsch et al., 1982, Fig. 11).

At 30–40 km distance phase a_1 is overtaken by phase a_3 with an apparent velocity clearly above 6 km/s. The corresponding retrograde phase a_2 is less clearly visible in the record sections because it immediately follows phase a_1 in secondary arrivals and is, therefore, disturbed by interference with the first-arrival phase. This retrograde phase a_2 is produced by a depth range with strong positive velocity gradient in which the velocity increases from 5.7 to 6.05 km/s. The position of the travel-time curve system a_0, a_0', a_1, a_2 and a_3 varies from profile to profile indicating lateral variations within the upper crust (see also Jentsch et al., 1982).

Also, the amplitudes of phase a_3 characteristically vary through the area of investigation. On most profiles the energy of those phases decreases considerably between 50 and 70 km distance and may even vanish completely (see more

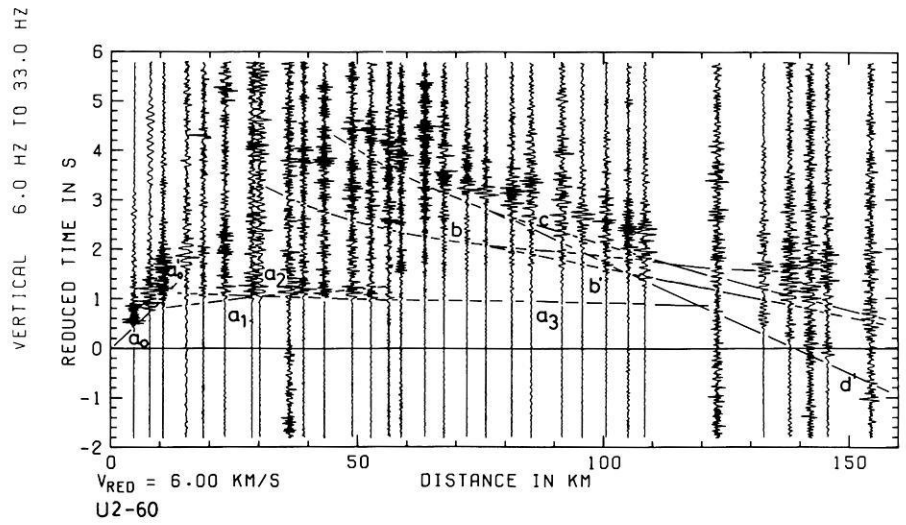

Fig. 2. Record section of the seismic refraction profile U2-60 observed from shotpoint U2 towards ENE (azimuth of 60°). a_o, a_1, a_3, b', d' refracted phases. a'_o, a_2, b, c reflected phases. The travel-time curves were calculated from the model of Fig. 6

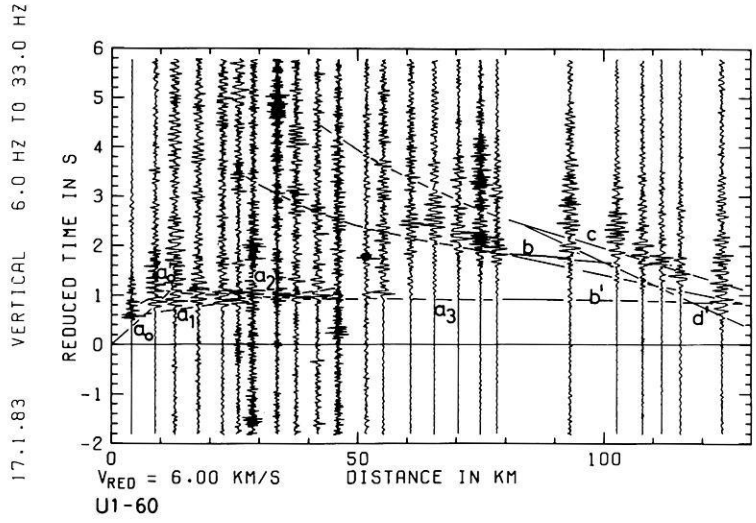

Fig. 3. Record section of the seismic refraction profile U1-60 observed from shotpoint U1 towards ENE (azimuth of 60°). For further explanations, see Fig. 2

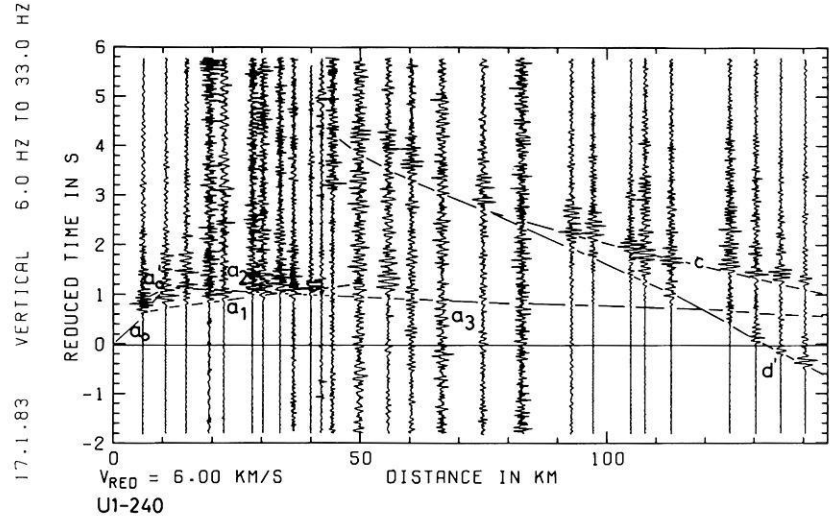

Fig. 4. Record section of the seismic refraction profile U1-240 observed from shotpoint U1 towards WSW (azimuth of 240°). For further explanations, see Fig. 2

detailed discussion below). It is explained by the existence of a pronounced low-velocity zone in the middle crust.

The lower boundary of this zone of velocity inversion in the middle crust is fixed by the retrograde travel-time branch of phase *b*. This phase varies from strong to weak appearance in the record sections and is completely lost on profiles U1-240 and U2-240. On the other hand, phase a_3 can clearly be correlated to larger distances. Both observational features indicate that the low-velocity area terminates towards WSW. The variability of the amplitudes and

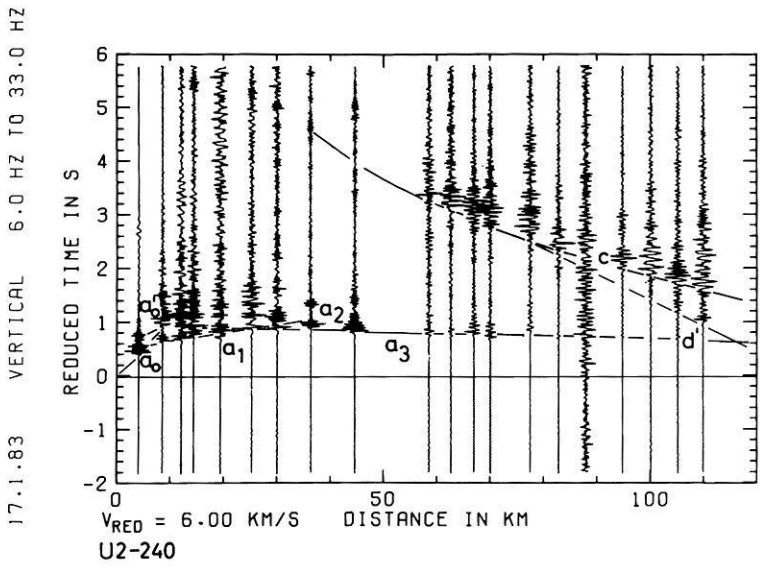

Fig. 5. Record section of the seismic refraction profile U2-240 observed from shotpoint U2 towards WSW (azimuth of 240°). For further explanations, see Fig. 2

of the travel time of phase *b*, where it exists, are explained by a strongly varying topography of the lower boundary of the low-velocity zone. For example, note the strong amplitudes of this phase on profile U1-60 in the distance range 50–80 km.

A prograde travel-time branch *b'* cannot safely be correlated. Either it does not exist or it is very weak and therefore hidden in the signal-generated noise of other phases. This leads to the conclusion that below the boundary determined by curve *b* the velocity gradient is only slightly positive or even negative.

On all record sections a phase *c*, interpreted as reflection from the crust-mantle boundary (commonly named P^MP, P_MP or P_mP), can be clearly correlated over a wide distance range between 50 and 140 km. Only the profile U1-60 seems to be an exception. On the other hand, its apparent weakness could also be caused by the existence of the strongly developed phase *b* to which the amplitudes in this distance range are normalized. The critical distance of phase *c* is generally between 55 and 70 km shotpoint distance.

The records of Figs. 2–5 clearly indicate the existence of first arrivals which can be correlated as phase *d'* with apparent velocities of 8.0–8.2 km/s and which are interpreted as the P_n phase penetrating into the uppermost mantle. The strong increase of amplitudes of the P_n phase at distances > 120 km is probably caused by a positive velocity gradient within the underlying uppermost mantle. Or it may even be caused by the existence of an increasing velocity gradiant, which may lead to the occurrence of a retrograde phase d_1 with apparent velocities of up to 8.4 km/s. This, however, is difficult to distinguish from the prograde phase *d'* (see also Ansorge et al., 1979; Stangl, 1983).

All profiles of sufficient recording length with azimuths between 40° and 60° show these clear P_n amplitudes and high apparent velocities. Unfortunately, most profiles except the main line with azimuth 60° or 240° were quite short and consequently, e.g. on the profile 30–80 (see Fig. 1), a P_n phase could not be identified. Therefore, it is not possible to investigate the amplitude and velocity characteristics of the P_n phase in greater detail with respect to observational direction (Bamford, 1973; Fuchs, 1983).

The crustal model

For each profile a velocity-depth function was derived assuming that the velocity varies only with depth. For the profiles along the 60°-line from these velocity-depth functions, isolines of equal velocity were constructed leading to a first-approximation two-dimensional model. This served as a starting model for a ray-tracing procedure (Červený et al., 1977) varying the initial model until the theoretical travel times fitted the observed ones. In addition, the observed amplitudes were considered. As a result – but with the limitations of the first-order ray theory – kinematically and dynamically controlled two-dimensional velocity-depth distributions could be derived for the 60°-line (Fig. 6). More details of this procedure are described by Gajewski and Prodehl (1983). The velocity distribution is presented by lines of equal velocity. Boundary zones are indicated by a great density of velocity isolines, first-order discontinuities by superposition of several isolines.

The crystalline crust is covered by sediments in which the average velocity increases gradually with depth from 3.8 km/s near the surface to about 4.7 km/s at the basement, where it jumps discontinuously to about 5.5 km/s. Details of the structure of the crystalline basement and variations of its surface are described by Jentsch et al. (1982).

The most prominent feature of the crustal model shown in Fig. 6 is a low-velocity zone between 8 and 19 km depth which extends over 100 km in a horizontal direction and has a maximum thickness of 10 km. It terminates to the WSW near the Hohenzollerngraben and to the ENE near the Nördlinger Ries. The average velocity within this zone is 5.8 km/s.

The upper crust above this low-velocity zone is characterized by a strong velocity gradient. At about 3–5 km depth the velocity increases quite abruptly from 5.7 to 6.05 km/s.

At the lower boundary of the low-velocity zone the velocity increases discontinuously from 5.8 to 6.6 km/s. The lower crust, with an average velocity of 6.7 km/s, is between 8 and 11 km thick below and ENE of the low-velocity zone, but thins drastically west of the Hohenzollerngraben.

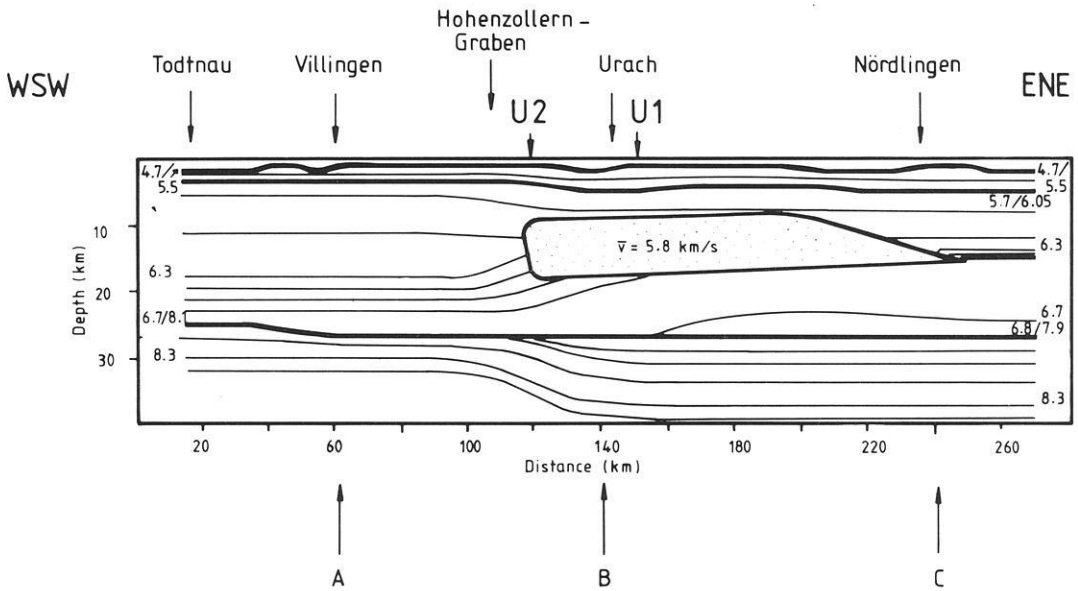

Fig. 6. Crustal model of the main profile observed through the Urach geothermal anomaly in a WSW-ENE direction. The contour interval of the lines of equal velocity is 0.1 km/s. Velocities <5.6 km/s are not shown. Depth scale is exaggerated 2:1 vs distance scale. *Dotted area*: zone of reduced velocity. *Arrows* A, B, C refer to velocity-depth functions of the respective model in Fig. 14

The termination of the low-velocity zone to ENE and to WSW is not well constrained. As mentioned above, the shotpoint distribution is not ideal for investigations of the whole crust, in particular when such lateral variations exist. As a consequence, details of the position and the shape of the boundaries of the low-velocity zone in the middle crust towards ENE and WSW can be modelled in various ways without contradicting the observed data. The WSW boundary, especially, has been studied in more detail and Fig. 6 shows a possible model which seems to fit the observed travel-times and amplitudes best.

The 6.3–6.6 km/s isolines rise in the area of the Hohenzollerngraben and join there to form the bottom of the low-velocity zone.

The crust-mantle boundary is a first-order discontinuity. WSW, towards the Rhinegraben, it is located at 25 km depth. Towards ENE, it drops to 26.5 km under the Swabian Jura. In the same direction the velocity jump at the Moho changes from 6.7/8.1 to 6.7/7.9 km/s.

The model does not only show strong lateral variations with respect to the existence of the low-velocity zone, which is restricted to the Urach geothermal anomaly zone, but is also quite different WSW and ENE of this zone. The boundary between upper and lower crust towards the Black Forest is much more transitional.

Also, the uppermost mantle shows lateral variations of velocity reaching up to 8.4 km/s and a strong increase of velocity with depth (Ansorge et al., 1979; Stangl, 1983).

Amplitude characteristics

For the profiles U1-60, U2-60, U2-240 and U1-240 (Figs. 2–5) along the main line, ray theoretical synthetic seismograms have been calculated based on the model in Fig. 6 (Figs. 7–10). Basically, the calculation of synthetic seismograms is more exact if the reflectivity method (Fuchs and Müller, 1971) is used which, in addition to amplitude studies, allows the study of frequency variations, e.g. such as the shift of the critical distance as a function of frequency. However, this method can, at present, only be applied for structures which change in vertical but not horizontal direction. For our problem, with vertically and laterally changing structures, only the ray theory could be applied using programs developed by Červený, Pšenčik and co-workers (e.g. Červený et al., 1977; Červený and Pšenčik, 1982).

Note that the distance axes of the observed record sections (Figs. 2–5) are numbered differently from those of the synthetic record sections (Figs. 7–10). The synthetic record sections use the same distances as are shown for the model in Fig. 6: shotpoint U2 corresponds to model-km 120, shotpoint U1 to model-km 150. Depending on the azimuth, distances increase (azimuth 60°, towards ENE) or decrease (azimuth 240°, towards WSW). All ray theoretical record sections are reduced with 6 km/s and show vertical components of ground displacement.

For the following reasons it did not seem reasonable to aim for an exact amplitude agreement of synthetically calculated and observed phases. Firstly, such a trial is prohibitive because of the limitations of the ray method. Secondly, the observed amplitudes are not only influenced by the deeper structure of the earth's crust, but are disturbed by many near-surface features as well as biased by instrumentally caused uncertainties. Rather, the aim was to explain the observed data qualitatively. This is best obtained by concentrating on the amplitude relations of various phases within the same seismogram.

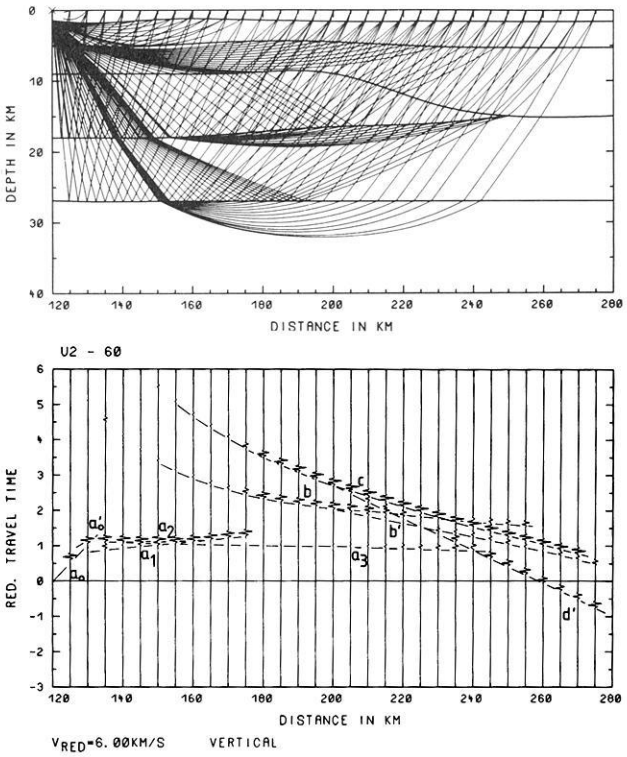

Fig. 7. Ray diagram for the model of Fig. 6 (*top*) and ray theoretical synthetic seismograms for shotpoint U2 (model-km 120) observed towards ENE (azimuth of 60°) with normalized amplitudes. The *heavy lines* in the ray diagram represent discontinuities of the model. Identification of phases corresponds to that of Figs. 2–5

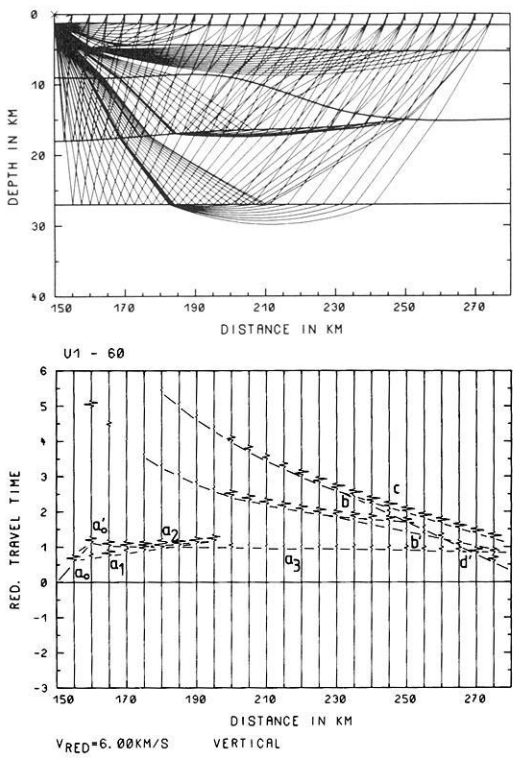

Fig. 8. Ray diagram for the model of Fig. 6 and ray theoretical synthetic seismograms for shotpoint U1 (model-km 150) observed towards ENE (azimuth of 60°), plotted with normalized amplitudes. The *heavy lines* in the ray diagram represent discontinuities of the model. Identification of phases corresponds to Figs. 2–5

The upper part of Figs. 7–10 contains ray diagrams for the corresponding profiles shown in Figs. 2–5. They show individual receiver positions along the profiles and the corresponding rays traversing the earth's crust. In the lower part of the figures the corresponding ray theoretical seismograms are shown. The synthetic seismograms are normalized in the same way as the observed data in Figs. 2–5.

The comparison of observed and computed seismograms (Figs. 2–5 and 7–10, respectively) shows pretty good agreement. All essential observed phases are also documented in the synthetic data and the amplitudes fit quite well too. If, on a seismogram, only one phase appears, the normalization procedure will amplify that phase, which in some cases may be irritating. Also, it may happen that the true amplitudes of the observed seismograms are larger than the ones on the adjacent traces. Then the synthetic section differs visually from the observed one even if more than one phase is seen on each seismogram. For example, this is the case for phase *b* which apparently increases in amplitude in the near-vertical reflection range (Fig. 7).

In the synthetic sections shown in Figs. 7–10, phases a_1 and a_2 cannot easily be distinguished because the two phases interfere with each other. In the observed seismograms, also, these phases cannot easily be separated because they follow each other with only a 0.2-s time difference.

For phase a_3, in any case, this leads to sufficient agreement of synthetic and observed data. Looking at the ray diagrams (Figs. 7 and 8), one recognizes that the rays of these arrivals penetrate the depth range below 5 km but still above the low-velocity zone, an area with a relatively small velocity gradient. Minor changes in the model parameters, e.g. shifting the upper surface of the low-velocity zone by only a few hundred metres, have significant consequences on this phase a_3, because this considerably changes the distance at which some energy of this phase can still be observed. According to ray theory, a phase always disappears abruptly if caused by a low-velocity zone or a caustic region.

For profile U1-60 the agreement between observed (Fig. 3) and synthetic (Fig. 8) data is not so good, because the computed amplitude relations of phases *b* and *c* in the middle distance range do not fit the character of the observed records very well.

Ray theory always results in too small a value for the critical distance (caused by high-frequency approximation). For crustal investigations this shift of the critical distance towards smaller values is between 10 km and some tens of kilometres (Červený et al., 1977). As the frequencies of phases *b* and *c* are quite similar, however, this effect would shift the critical distance of both phases together so that the amplitude relation should not be altered by this effect.

So it can only be concluded that the reason for the disagreement between computed and observed record sections for profile U1-60 must be caused by the low-velocity zone rather than by the structure of the Moho. With the exception of this particular profile U1-60, all other profiles show clear P^MP energy at distances greater than 50 km. In addition, the vertices of the rays of the reflection from the Moho on profile U2-60 are only 30 km from those on profile U1-60. The rays for both profiles penetrate through

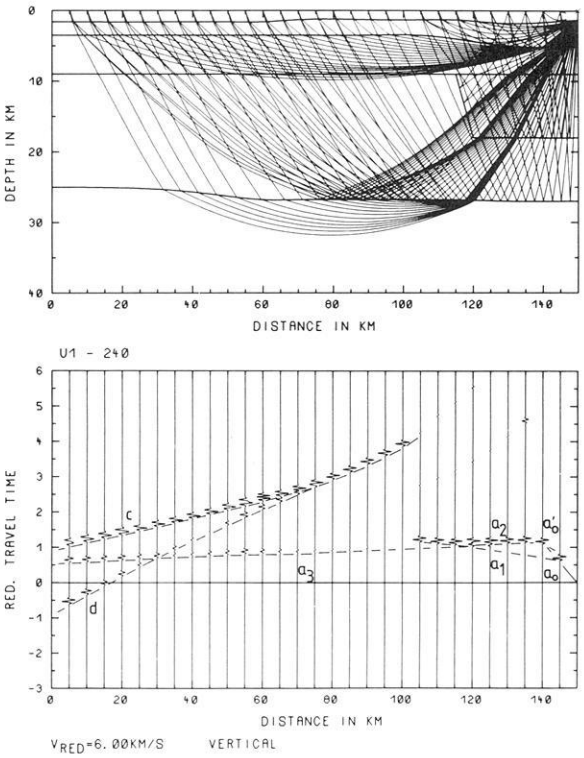

Fig. 9. Ray diagram for the model of Fig. 6 and ray theoretical synthetic seismograms for shotpoint U1 (model-km 150) observed towards WSW (azimuth of 240°), plotted with normalized amplitudes. For further explanations, see Fig. 8

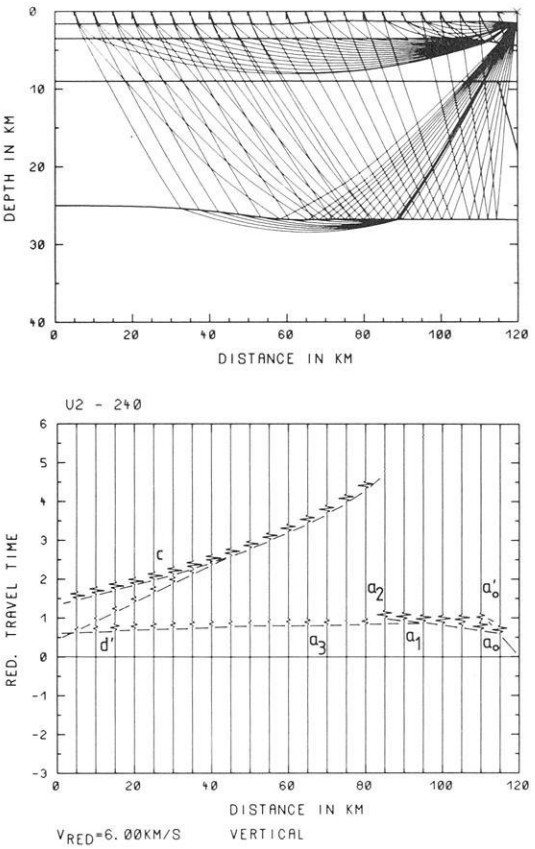

Fig. 10. Ray diagram for the model of Fig. 6 and ray theoretical synthetic seismograms for shotpoint U2 (model-km 120) observed towards WSW (azimuth of 240°) plotted with normalized amplitudes. For further explanations, see Fig. 8

the low-velocity zone, but only one profile, U2-60, shows "normal" amplitude characteristics for the P^MP phase. It is unreasonable to assume that the Moho changes drastically within this 30-km horizontal distance, which would be necessary to shift the critical distance by more than 50 km.

The only reasonable solution, therefore, seems to assume strong lateral variations within the low-velocity zone itself. The assumed mean velocity of 5.8 km/s is an average value which certainly may be larger or smaller locally. Unfortunately, the seismic refraction data do not allow any definite conclusions with respect to this problem.

The synthetic data of profiles U1-240 and U2-240 again agree quite well with the observed data (Figs. 4 and 5 and Figs. 9 and 10.).

For both profiles, it is evident that in the observed and the computed record sections phase *b* is missing. On the other hand, the synthetic data of profile U1-240 show some energy resulting from reflections from the flanks of the low-velocity zone as can be seen in the ray diagram (Fig. 9, upper part). Such arrivals are also weakly seen in the observed data. The energy of that phase is quite low and, therefore, almost hidden by signal-generated noise in the data. The amplitude characteristics of phases *c* and *d'* (P^MP and P_n) are well demonstrated by the synthetic data, only phase a_3 terminates too late in the computed sections.

In summary it can be concluded that, in general, good agreement could be reached between observed and computed amplitude data. Exceptions are caused mainly by influences of the low-velocity zone. Thus, it has to be assumed that this low-velocity zone possesses laterally varying fine structure which, however, cannot be resolved. Based on the amplitude information of the P^MP and P_n phases, no indication of a stronger absorption within the low-velocity zone can be seen. Also phase *b*, the reflection from the bottom of this zone, does not allow any conclusions in that respect.

Comparison with results of the seismic reflection experiments

The model resulting from the interpretation of the near-vertical seismic reflection experiment (Bartelsen et al. 1982), located on a profile approximately 20 km NW of our 60° line (Figs. 1 and 15), is reproduced in Fig. 11. The complementary model based on wide-angle measurements along the same line of the near-vertical reflection observations was prepared by Trappe (1983) and is reproduced in Fig. 12. A direct comparison of the three models (Figs. 6, 11 and 12) is difficult because the model of the near-vertical reflection survey consists of layers with constant interval velocity, while the models of our seismic refraction survey and that from the wide-angle observations of the reflection line use velocity gradients, i.e. the velocity increases with increasing depth between velocity isolines. Nevertheless, the characteristic features can be compared.

All models show a low-velocity zone with a mean veloci-

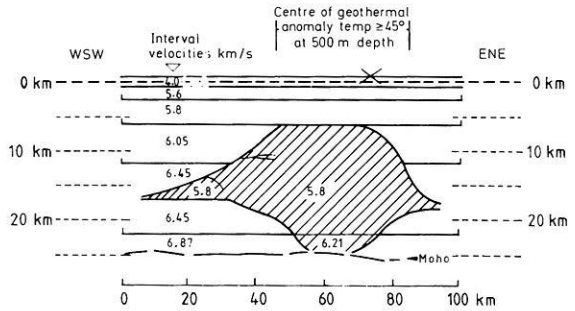

Fig. 11. Crustal model of Bartelsen et al. (1982, Fig. 13) of the Urach geothermal anomaly derived along the WSW-ENE seismic reflection line (Fig. 1) from near-vertical reflection observations

ty of 5.8 km/s. The extension in the horizontal direction differs. This may be caused by the difference in location (Fig. 15). The surface of this low-velocity zone of the "near-vertical" model (Fig. 11) is found at only 6 km depth, while that of the "wide-angle" model along the same line lies at about 9 km depth (Fig. 12) and thus corresponds to our result (Fig. 6) including the rise of this boundary towards ENE.

Bartelsen et al. (1982) concluded that this boundary could be interpreted as a transitional layer or as a lamellar structure with thin alternating low- and high-velocity layers, because they were able to prove the existence of horizons with increasing and decreasing impedance, at least in the WSW part of their line. On the other hand, no near-vertical reflections could be found from the top of the low-velocity zone in its central part.

So, the above-mentioned difference in depth may not be significant. In any case, it cannot be explained by different profile locations because the "near-vertical" model (Fig. 11) and the "wide-angle" model were derived for the same line. The agreement of the "wide-angle" model (Fig. 12) and our model (Fig. 6), for the upper crust including the low-velocity zone, is extremely good. This also holds for the structure and depth of the Moho. Significant deviations do exist for the crustal depth range immediately below the low-velocity zone. The velocities here are quite different. Only at the WSW and ENE "edges" of the models is the average velocity of all models approximately equal. With respect to the unfavourable shotpoint distribution of our experiment, the greatest uncertainties have to be faced here.

Figure 13 summarizes the results of all profiles in a fence diagram, including the seismic reflection line. As none of the profiles outside the 60°-line was reversed or overlapped, it is almost impossible to determine the three-dimensional extensions of the low-velocity zone.

A pronounced change in crustal structure is observed on the profiles pointing towards the Rhinegraben. In comparison to the crust east of the low-velocity zone, the lower crust in the west is thinner. The rise of the Moho towards the Rhinegraben may be connected with the general uplift of the graben and its shoulders (Edel et al., 1975; Giese, 1976), the distance between Urach and Rhinegraben being less than 100 km.

Comparison with crustal structure results of adjacent areas

For the adjacent areas a number of quite recent investigations exist (Deichmann and Ansorge, 1983; Stangl, 1983; Strössenreuther, 1982; Zucca, 1984) which complement the earlier publications (Aichele, 1976; Edel et al., 1975; Emter, 1971; Mueller et al., 1973; Prodehl et al., 1976).

Figure 14 shows velocity-depth functions of our two-dimensional model (Fig. 6) for three selected positions (Fig. 14a–c). The lower part of Fig. 14 shows some velocity-depth functions of other observations west (Fig. 14d) and east (Fig. 14e) of our area of investigation. The location of these surveys is shown in Fig. 15.

The models of Aichele (1976) and Strössenreuther (1982) show zones of velocity inversions with an average velocity of 5.8 km/s and around 10 km depth (Fig. 14e). Their low-velocity zones, however, are thinner than that in the centre of the Urach area (Fig. 14b).

Profile 09-240 is the continuation of our 60°-line into the Franconian Jura (Fig. 15). Contrary to the results of Aichele and Strössenreuther, Stangl (1983) does not find any velocity inversion from this profile. His model is quite similar to our velocity-depth function at model-km 240 (Fig. 14c and e). However, shotpoint 09 is more than 200 km from shotpoint U1 and, consequently, the turning points of corresponding rays are more than 100 km apart.

In conclusion, the area of the Swabian and Franconian Jura shows strong lateral variations of the crust. A discontinuity or transition zone at depths between 15 and 20 km in the middle crust seems to be typical for the South German Jura mountains (see Fig. 14e). It is not clear whether the low-velocity zone under the anomalous region of Urach is related to the one stated by Aichele (1976) and Strössenreuther (1982) for the Franconian Jura. Information is lacking on the crust under the area in between these two regions.

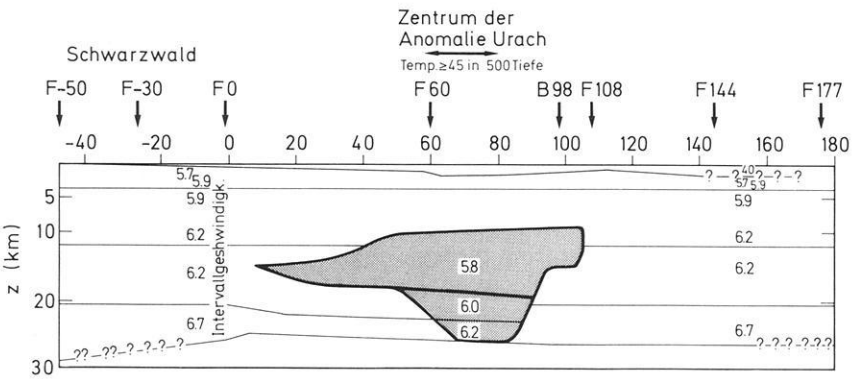

Fig. 12. Crustal model of Trappe (1983, Fig. 53) of the Urach geothermal anomaly derived along the WSW-ENE seismic reflection line (Fig. 1) from wide-angle reflection observations

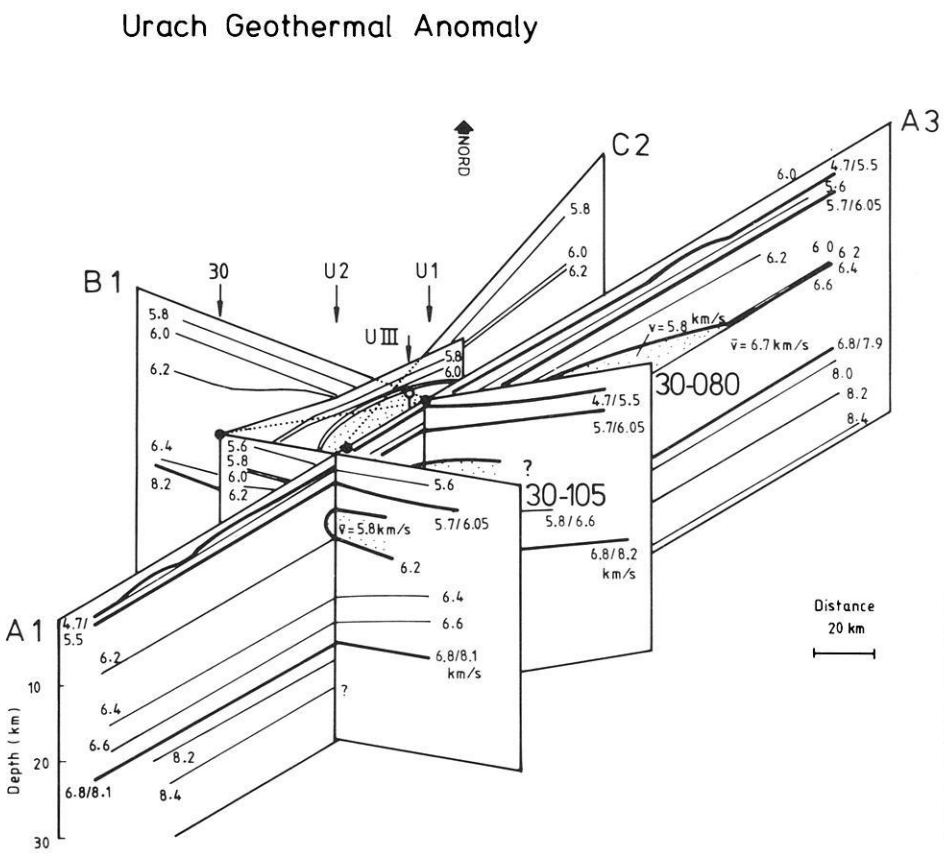

Fig. 13. Fence diagram showing the crustal structure in the area of the Urach geothermal anomaly based on seismic refraction and reflection measurements. Depth is exaggerated 2.3:1 vs horizontal distance. The contour interval of lines of equal velocity is 0.2 km/s. Velocities <5.6 km/s are not shown. *Dotted area* indicates the position of a low-velocity zone

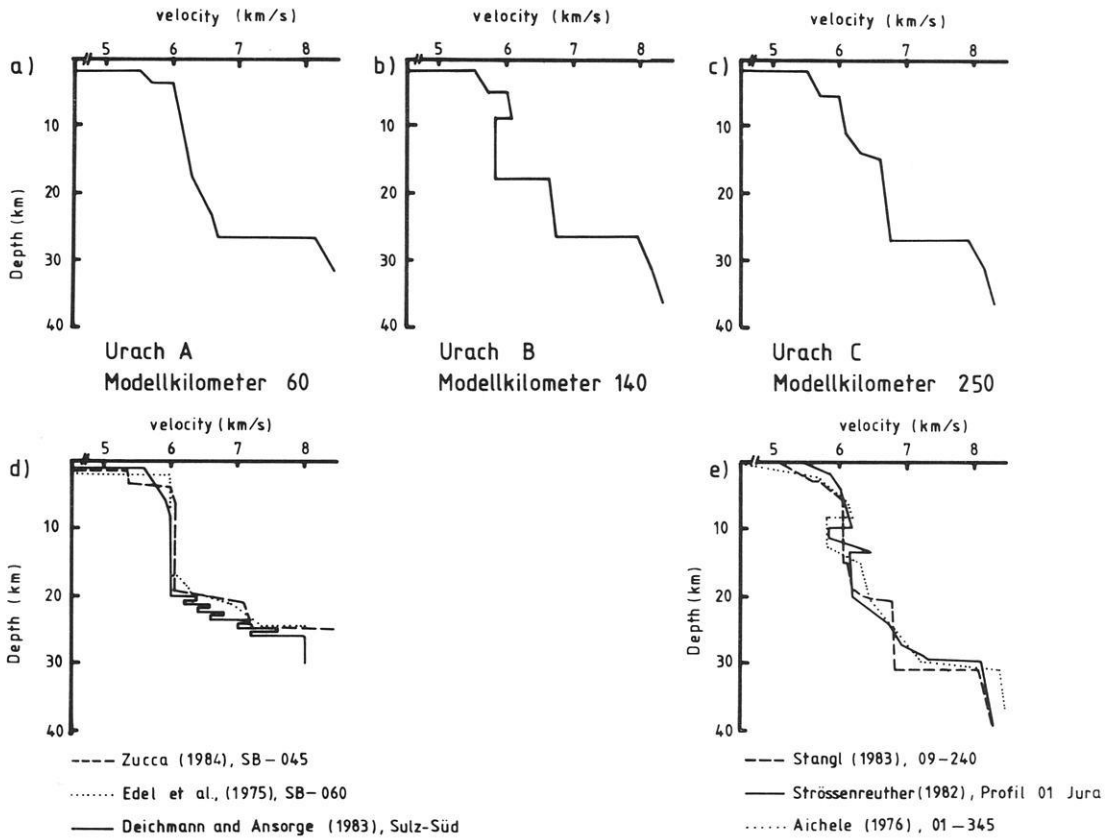

Fig. 14a–e. Velocity-depth functions representing various areas of the Urach geothermal anomaly (**a–c**) according to the model of Fig. 6 and adjacent areas to the west (**d**) and to the east (**e**)

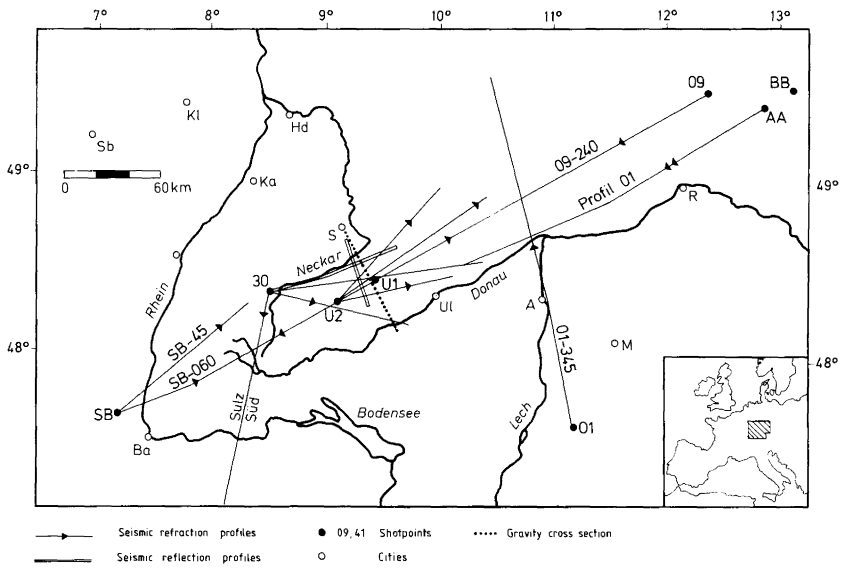

Fig. 15. Location map of seismic refraction and reflection profiles and a gravity cross-section in southwest Germany mentioned in Figs. 14 and 16 and in the text

Discussion and conclusions

The interpretation of a series of seismic refraction profiles in the area of the Urach geothermal anomaly has proved the existence of a low-velocity zone ($\bar{v}=5.8$ km/s) in the middle crust. How can such a zone be interpreted?

A gravimetric profile, oriented approximately perpendicular to our 60°-line and crossing it near shotpoint U1 (Figs. 15 and 16), shows a high-density body in the area of the geothermal anomaly (Makris et al., 1982), in apparent contrast to the existence of the low-velocity zone found by reflection and refraction seismics. The density contrast of that body with respect to the surrounding crustal material is up to 0.26 g/cm^3, depending on the particular model of Makris et al. (1982). In this connection, the absence of near-vertical reflections from the surface of the low-velocity zone is of particular interest. According to the model of Bartelsen et al. (Fig. 11) it means that the velocity does not change here. On the other hand, both the "wide-angle" model of Trappe (Fig. 12) and our model (Fig. 6) do show *P*-wave velocities of up to 6.1–6.2 km/s above the low-velocity zone. This is not in contradiction to the seismic reflection result which gives interval velocities, i.e. an average velocity for the layer above the low-velocity zone.

A possible explanation for the fact that no near-vertical reflections are observed from the top of the low-velocity zone is that the impedance, i.e. the product of *P*-velocity and density, does not change. As the *P*-wave velocity is reduced from 6.2 to 5.8 km/s, the density must increase if the impedance is to remain constant. One can determine the density corresponding to 6.2 km/s after Nafe and Drake (see Talwani et al., 1959) and then compute the corresponding impedance. From that and the velocity of 5.8 km/s, a density of 3.0 g/cm^3 results for the low-velocity body and a density contrast of $\Delta\rho=0.21$ g/cm^3 with respect to the overburden. This contrast is within the range given by Makris et al. (1982) (Fig. 16).

Such an interpretation can explain both the decrease of seismic velocity and the increase of Bouguer gravity for the Urach geothermal anomaly. The combination of such high density and low *P*-wave velocity requires the existence of fluid or gas phases or partial melting of the rocks concerned (e.g. gabbro). This, however, leads to much higher temperatures in this depth range than has been assumed until now (e.g. Haenel and Zoth, 1982).

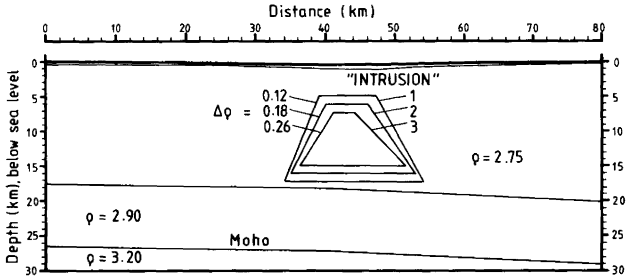

Fig. 16. Density model of Makris et al. (1982, Fig. 4) for a line crossing the Urach geothermal anomaly from NNW to SSE, perpendicular to the seismic lines of Figs. 2–12. For position of gravity cross-section, see Fig. 15

The assumption of the existence of partially molten material or fluid or gas phases is supported by an investigation of *S* waves. While clear wide-angle *P*-wave reflections from the lower boundary of the low-velocity zone can be observed on all profiles concerned (phase *b* in Figs. 2–4), *S*-wave reflections cannot be detected on any of the profiles as shown, for example, for profile U1-60 (Fig. 17). The record section is reduced with 3.46 km/s (corresponding to $V_P/V_S=\sqrt{3}$). The time scale is chosen so that the full range of observed *P* and of expected *S* phases can be detected. The full lines show the travel-time curves of the *P* waves and are the same as shown in Fig. 3. Dotted lines are travel-time curves of *S* waves calculated from the *P*-wave travel-times assuming a Poisson's ratio of 0.25, i.e. $V_P/V_S=\sqrt{3}$.

Figure 17 clearly demonstrates that there is no *S* wave recorded as a reflection from the bottom of the low-velocity zone. Also, the S^MS phase, the *S*-wave reflection from the Moho, and the corresponding S_n wave, refracted in the uppermost mantle, cannot be seen in the record sections. The result is the same for the record sections of the horizontal components. While shotpoint U1 does not show any *S* energy from the middle and lower crust, a weak S^MS

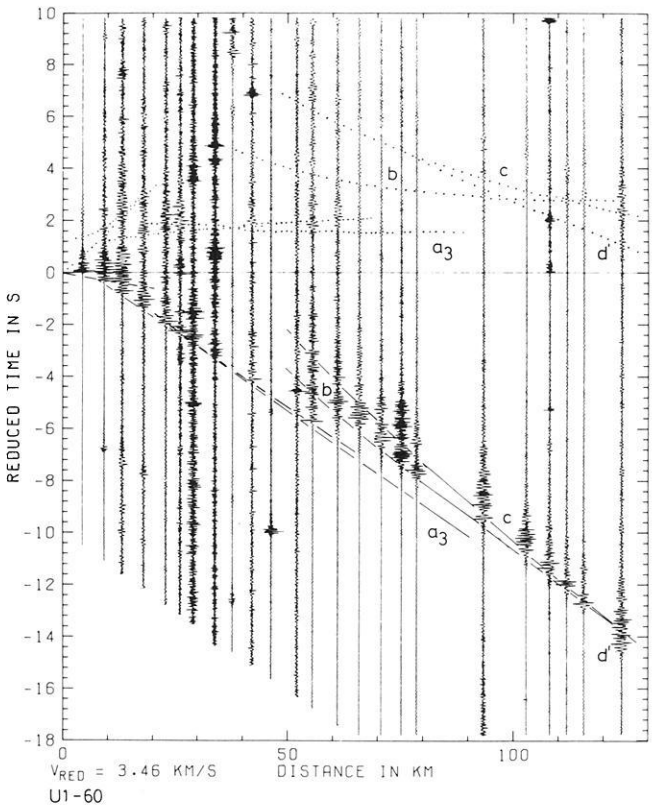

Fig. 17. Record section of the seismic refraction profile U1-60. Reduction velocity = 3.46 km/s. *Solid lines* are the travel-time curves calculated for P waves from the model of Fig. 6 and are the same as shown in Fig. 3. *Dotted lines* are travel-time curves for S waves calculated from the same model and assuming a Poisson's ratio of $P_P/V_S = \sqrt{3}$

phase is observed for shotpoint U2 in both directions. Its energy is considerably smaller than the corresponding P^MP-phase energy in ENE direction, but stronger to the WSW. This is probably caused by the fact that, on this profile, the rays penetrate the low-velocity zone only on half of their total ray path.

As partial melts attenuate S waves stronger than P waves (Mavco, 1980), these observations may be a further indication for the existence of such partial melt.

If one explains the low-velocity zone with high density as magmatic intrusion, then this event should have happened about 1 million years ago according to a simple heat conduction model calculation (Lachenbruch et al., 1976; Chapman, personal communication), in order to preserve temperatures of about 700° C until present times. Such short time span, however, does not correspond with the occurrence of the known volcanic activity which happened about 15 million years ago in this area.

Considering the total crustal thickness, a rather thin crust exists under the Urach geothermal area which is similar to that found under the Rhinegraben proper, 60–80 km to the west. Taking into account the results of the profile Sulz-S (Deichmann and Ansorge, 1983) and the profiles extending from the Rhinegraben into the Black Forest (Edel et al., 1975), it seems that the crust remains shallow throughout the whole area between the Black Forest and the Swabian Jura, in contrast to the increase of crustal thickness west of the Rhinegraben. According to Aichele (1976) and Strössenreuther (1982), the standard central European crustal thickness of about 30 km is present under the Franconian Jura, so that the transition must be located somewhere near the Nördlinger Ries.

In conclusion, the seismic investigations of the geothermal anomaly of Urach reveal a rather heterogeneous crustal structure. Beneath the centre of the anomaly a well constrained low-velocity zone is found whose extension coincides fairly well with the contours of the isolines of geothermal gradient. Though its exact western and eastern extension cannot be accurately fixed it can be stated that its western border coincides approximately with the position of the Hohenzollerngraben, a fracture zone which is cut by a N-S trending line of major anomalous earthquake activity.

The combination of gravity and seismic data may indicate the existence of partial melts of high density which may not be older than about 1 million years, in contrast to the known volcanic activity in this area which occurred about 15 million years ago.

The fact that the crust is almost as thin as that beneath the Rhinegraben proper may suggest that either the same anomalous mantle is present under the whole area reaching from the Rhinegraben to the Urach area or that two branches of anomalous mantle behaviour exist.

Acknowledgements. The investigation, as part of a multidisciplinary project under the responsibility of Dr. Ralph Haenel, Hannover, was jointly sponsored by the European Community (contract no. 071-76 EG 61A-23-5) and the Federal Ministry for Research and Technology (contract no. EG 4027A). The interpretation work was additionally supported by the German Research Association with the special research programme "Stress and stress release in the lithosphere" of the University of Karlsruhe (SFB 108).

We are grateful to K. Fuchs (Karlsruhe), D. Chapman (Clausthal, on leave from Salt Lake City), P. Giese (Berlin) and H. Wilhelm (Karlsruhe) for fruitful discussions. The Institute of Geophysics of the University of Kiel supplied original data and figures. W. Kaminski helped intensively during the digital data preparation on the Raytheon 500 computer of the Geophysical Institute of the University of Karlsruhe. Beate Aichroth and W. Friederich carried out many calculations which were performed on the Burroughs 7700 computer of the Computer Centre of the University of Karlsruhe.

References

Aichele, H.: Interpretation refraktionsseismischer Messungen im Gebiet des Fränkisch-Schwäbischen Jura. Ph.D. Thesis, University of Stuttgart, 1976

Ansorge, J., Bonjer, K.-P., Emter, D.: Structure of the uppermost mantle from long-range seismic observations in southern Germany and the Rhinegraben area. Tectonophysics **56**, 31–48, 1979

Bamford, D.: Refraction data in western Germany – a time-term interpretation. J. Geophys. **39**, 907–927, 1973

Bartelsen, H., Lueschen, E., Krey, Th., Meissner, R., Schmoll, H., Walter, Ch.: The combined seismic reflection-refraction investigation of the Urach geothermal anomaly. In: The Urach geothermal project, Haenel, R. ed.: pp 231–245, Schweizerbart, Stuttgart, 1982

Carlé, W.: Die Wärme-Anomalie der mittleren Schwäbischen Alb (Baden-Württemberg). In: Approaches to Taphrogenesis, Illies, H.J., Fuchs, K., eds: pp 207–212, Schweizerbart, Stuttgart, 1974

Červený., Molotkov, I.A., Pšenčik, I.: Ray method in seismology, Univerzita, Karlova, Prag, 1977

Červený, V., Pšenčik, I.: Seismic ray package, Fortran program. Prag, 1982

Deichmann, N., Ansorge, J.: Evidence for lamination in the lower continental crust beneath the Black Forest (southwest Germany). J. Geophys. **52**, 109–118, 1983

Dietrich, H.-G.: Geological results of the Urach 3 borehole and the correlation with other boreholes. In: The Urach geothermal project, Haenel, R., ed.: pp 49–58, Schweizerbart, Stuttgart, 1982

Edel, J.B., Fuchs, K., Gelbke, C., Prodehl, C.: Deep structure of the southern Rhinegraben area from seismic refraction investigation. J. Geophys. **41**, 333–356, 1975

Emter, D.: Ergebnisse seismischer Untersuchungen der Erdkruste und des oberen Erdmantels in Südwestdeutschland. Ph.D. Thesis, University of Stuttgart, 1971

Fuchs, K.: Recently formed elastic anisotropy and petrological models for the continental subcrustal lithosphere in southern Germany. Phys. Earth Planet. Inter. **31**, 93–118, 1983

Fuchs, K., Müller, G.: Computation of synthetic seismograms with the reflectivity method and comparison with observations. Geophys. J. R. Astron. Soc. **23**, 417–433, 1971

Gajewski, D., Prodehl, C.: Zweidimensionales seismisches Modellieren mit der Strahlenmethode. Berichtsband 1981–1983 des Sonderforschungsbereichs 108 der Universität Karlsruhe „Spannung und Spannungsumwandlung in der Lithosphäre", 209–227, 1983

Geyer, O.F., Gwinner, M.P.: Einführung in die Geologie von Baden-Württemberg. Schweizerbart, Stuttgart, 1968

Giese, P.: The basic features of crustal structure in relation to the main geologic units. In: Explosion seismology in Central Europe, Giese, P., Prodehl, C., Stein, A. eds.: pp 241–242, Springer, Berlin, Heidelberg, New York, 1976

Giese, P., Prodehl, C., Stein, A.: Explosion seismology in Central Europe. Springer, Berlin, Heidelberg, New York, 1976

Haenel, R. (ed.): The Urach geothermal project (Swabian Alb, Germany). Schweizerbart, Stuttgart, 1982

Haenel, R., Zoth, G.: Temperature measurements and determination of heat flow density. In: The Urach geothermal project, Haenel, R. (ed.): pp 81–88, Schweizerbart, Stuttgart, 1982

Illies, J.H.: Der Hohenzollerngraben und Intraplatten-Seismizität infolge Vergitterung lamellärer Scherung mit einer Riftstruktur. Oberrhein. geol. Abh. **31**, 47–78, 1982

Jentsch, M.: A compilation of data from the 1978–79 Urach, Baden-Württemberg, seismic-refraction experiment. Open-file report, 80-1. Geophys. Inst. Karlsruhe, 1980

Jentsch, M., Bamford, D., Emter, D., Prodehl, C.: A seismic refraction investigation of the basement structure in the Urach geothermal anomaly, southern Germany. In: The Urach geothermal project, Haenel, R. ed.: pp 247–262, Schweizerbart, Stuttgart, 1982

Lachenbruch, A.H., Sass, J.H., Munroe, R.J., Moses, T.H.: Geothermal setting and simple heat conduction models for the Long Valley caldera. J. Geophys. Res. **81**, 769–784, 1976

Makris, J., Müller, K., Tödt, K.H.: Gravity measurements at the geothermal anomaly Urach. In: The Urach geothermal project, Haenel, R. ed.: pp 313–322, Schweizerbart, Stuttgart, 1982

Mäussnest, O.: Die Eruptionspunkte des Schwäbischen Vulkans. Z. Dtsch Geol. Ges. **125**, 23–54, 277–352, 1974

Mavco, G.M.: Velocity and attenuation in partially molten rocks. J. Geophys. Res. **85**, 5173–5189, 1980

Meissner, R., Bartelsen, H., Krey, T., Schmoll, J.: Detecting velocity anomalies in the region of the Urach geothermal anomaly by means of new seismic field arrangements. In: Geothermics and geothermal energy, Čermák, V., Haenel, R., eds.: pp 285–292, Schweizerbart, Stuttgart, 1982

Mueller, S., Peterschmitt, E., Emter, D., Ansorge, J.: Crustal structure of the Rhinegraben area. Tectonophysics **20**, 381–391, 1973

Prodehl, C.: Crustal structure of the western United States. U.S. Geol. Survey Prof. Paper **1034**, 1979

Prodehl, C., Ansorge, J., Edel, J.B., Emter, D., Fuchs, K., Mueller, S., Peterschmitt, E.: Explosion-seismology research in the central and southern Rhinegraben – a case history. In: Explosion seismology in central Europe, Giese, P., Prodehl, C., Stein, A., eds: pp 313–328, Springer, Berlin, Heidelberg, New York, 1976

Prodehl, C., Emter, D., Jentsch, M.: Seismic refraction studies of the geothermal area of Urach, southwest Germany. In: Geothermics and geothermal energy, Čermák, V., Haenel, R., eds: pp 277–283, Schweizerbart, Stuttgart, 1982

Schädel, K.: The geology of the heat anomaly of Urach. In: The Urach geothermal project, Haenel, R., ed.: pp 147–156, Schweizerbart, Stuttgart, 1982

Schneider, G.: Seismizität und Seismotektonik der Schwäbischen Alb. Enke, Stuttgart, 1971

Stangl, R.: Geschwindigkeits-Tiefen-Verteilungen von P-Wellen im oberen Mantel Süddeutschlands, die mit Laufzeit- und Amplituden-Beobachtungen auf zwei gegengeschossenen Langprofilen verträglich sind. Diploma Thesis, University of Karlsruhe, 1983

Strössenreuther, U.: Die Struktur der Erdkruste am Südwestrand der Böhmischen Masse, abgeleitet aus refraktions-seismischen Messungen der Jahre 1970 und 1978/79. Ph.D.Thesis, University of München, 1982

Talwani, M., Sutton, G.H., Worzel, J.C.: A crustal section across the Puerto Rico Trench. J. Geophys. Res. **64**, 1545–1555, 1959

Trappe, H.: Eine Auswertung von Weitwinkelreflexionen auf dem Profil Urach und eine Korrelation zu den Ergebnissen der Steilwinkel-Reflexionsseismik. Diploma Thesis, University of Kiel, 1983

Turnovsky, J., Schneider, G.: The seismotectonic character of the September 3, 1978, Swabian Jura earthquake series. Tectonophysics **83**, 151–162, 1981

Zucca, J.J.: The crustal structure of the southern Rhinegraben from reinterpretation of seismic refraction data. J. Geophys. **55**, 13–22, 1984

Received December 19, 1983; Revised version October 15, 1984
Accepted October 16, 1984